Green synthesis of ferrous sulfide and magnesium sulfide nanoparticles and evaluation of their applications in photocatalytic degradation and antimicrobial activity

Elizabeth M. Kezia[1], Randhi Uma Devi[2*]

1 School of Science, GITAM Deemed to be University, Visakhapatnam, 530045, India
2 School of Science, GITAM Deemed to be University, Hyderabad, 502329, India
* Corresponding author's e-mail: urandhi@gitam.edu

ABSTRACT

This study explores the synthesis of metal sulfide nanoparticles (NPs) using *Hordeum vulgar* leaf extract as a sustainable green approach. The synthesized MgS and FeS NPs were characterized using UV-Vis spectroscopy analysis, X-Ray Diffraction, and SEM techniques. These nanoparticles exhibited significant efficacy in photocatalytic degradation of Rhodamine dye, achieving 95% degradation with 40 mg of MgS NPs and 10 mg of FeS NPs, indicating their potential for textile wastewater treatment. Moreover, the metal sulfide nanoparticles demonstrated antimicrobial activity against bacteria (*Staphylococcus aureus*, *Escherichia coli*) and fungi (*Aspergillus niger, Candida albicans*), suggesting their role in combating multidrug-resistant microbes. This research explores the promising applications of metal sulfide nanoparticles in combating textile pollution and focuses on sustainable environmental endeavours in agricultural practices opening new avenues for further research and development in this field.

Keywords: Green Synthesis, nano particles, *Hordeum vulgare*, anti-microbial agents, photocatalytic degradation.

INTRODUCTION

The discharge of large volumes of various dyes from diverse industries adversely affects aquatic organisms, plant life, and human health. Rhodamine B (Rh-B) is a highly water-soluble, basic dye belonging to the xanthene class. It is widely used as a fluorescent dye and colorant in textiles and food products (Richardson et al., 2004). Despite being valued in the textile industry for its stability and non-biodegradability, Rh-B is considered one of the most toxic dyes found in textile wastewater. However, Rh-B poses significant health risks to humans and animals due to its potential to cause skin, eye, and respiratory irritation. Additionally, Rh-B has been associated with carcinogenicity, reproductive and developmental toxicity, neurotoxicity, and chronic toxicity (Nagaraja et al., 2012; Hamdaoui, 2011). Urgent measures are required to mitigate the adverse effects of Rh-B, including regulatory actions to limit its use and improved wastewater treatment methods

to prevent environmental contamination (Sharma et al., 2024). Traditional wastewater treatment methods such as sedimentation, chemical flocculation, coagulation, filtration, and aeration are somewhat effective in removing dyes from textile effluents (Qin et al., 2024). However, these methods are associated with drawbacks including the production of toxic by-products like heavy metals, azo dyes, chlorobenzene and volatile organic chemicals like formaldehyde, high energy consumption, generation of odours, and the need for large treatment areas. Synthetic fibers from textiles can also shed microplastics during washing which can end up in environment and food chain and can cause potential harm to wild life and human health. These limitations have motivated researchers to seek more efficient technologies to improve the quality of textile wastewater treatment prior to discharge into the environment.

The rise of antimicrobial drug resistance (AMR) among microbial strains, coupled with a diminishing range of effective treatments,

presents a serious threat that could push the modern world back to a pre-antibiotic era where basic infections were often deadly (Kinch et al., 2024). Contributing factors to this issue include inadequate clean water, sanitation, and hygiene (WASH) practices for both humans and animals, along with deficiencies in healthcare facilities, limited awareness of AMR, and insufficient legislative enforcement (Crocker et al., 2024). *Staphylococcus aureus* (*S. aureus*) and *Escherichia coli* (*E. coli*) are common bacteria responsible for waterborne infections in humans, ranging from mild skin issues like boils to more severe conditions such as pneumonia, bloodstream infections (septicemia), and food poisoning (Agbasi et al. 2024). Water contamination with *Candida albicans* (*C. albicans*) and *Aspergillus niger (A. niger)* can occur in various ways, posing health risks to those exposed. Ingestion or inhalation of water containing *C. albicans* can result in gastrointestinal or respiratory infections, while water contaminated with *A. niger* can cause respiratory infections, particularly through aerosolized spores, especially for individuals with compromised immune systems or pre-existing lung conditions (Gnat et al., 2021). These pathogenic microorganisms can spread through contaminated water sources, emphasizing the importance of ensuring clean and safe drinking water through proper treatment and hygiene practices to minimize the risk of waterborne diseases (Forstinus et al., 2015).

Nanotechnology is a captivating field that enables the fabrication of extremely small objects and has made significant advancements in various industries including electronics, therapeutics, food production, sustainable agriculture, and environmental health (Azzazy et al., 2012). Innovative synthesis methods in nanomaterials have progressed through both top-down (*e.g.,* lithography, ball milling, etching, sputtering) and bottom-up (e.g., chemical vapor deposition, spray, sol-gel) approaches to control the dimensions, morphologies, and properties of nanomaterials (Gul et al., 2024; Kaur, 2024). There is a growing emphasis on ‚green synthesis' methodologies in advanced materials science and technology, which aim to produce environmentally friendly nanomaterials (Nanda et al., 2024). Green metallic nanoparticles derived from plant extracts offer sustainable alternatives to traditional synthesis methods, minimizing harmful byproducts and enhancing environmental protection (Alsaiari et., 2023). This research investigates the photocatalytic dye degradation and antimicrobial effects of environmentally friendly *Hordeum vulgare* (barley) magnesium sulfide (MgS) and ferrous sulfide (FeS) nanoparticles, demonstrating their potential for efficient pollutant removal and antimicrobial activity in environmental applications.

METHODOLOGY

Synthesis phyto capped MgS and FeS NPs

MgS nanoparticles were synthesized by adding an extract from *Hordeum vulgare* leaves to equal portions of 1M aqueous solutions of $Mg(NO_3)_2$ and Na_2S. The leaves of the Hordeum vulgare plant extract are combined with 50 ml of a 1M aqueous solution of $Mg(NO_3)_2$ in a beaker and heated at 40 °C for 50 minutes. Simultaneously, a second beaker containing 50 ml of a 1M aqueous Na_2S solution is stirred at 40 °C for 50 minutes. After agitation, 25 ml of Hordeum vulgare leaf extract is combined with 25 ml of 1M aqueous solutions of $Mg(NO_3)_2$, and 50 ml of 1M aqueous solutions of Na_2S is slowly added using a burette to precipitate Hordeum vulgare leaf extract-capped MgS nanoparticles. Capped magnesium sulfide nanoparticles from *Hordeum vulgare* leaf extract are produced using a separating funnel and filter paper. To fully clean the precipitate, ethanol and distilled water were used before heating it to a temperature of 80 °C for 5 hours in a hot air oven. After drying, the sample was crushed with a mortar and pestle to produce a fine powder. The same method followed to synthesize FeS nanoparticles using Ferrous nitrate $[Fe(NO_3)_3]$ and sodium sulfide (Na_2S) in an aqueous solution. The resulting products as a fine powder after crushing the dried sample with a mortar and pestle were characterized. UV-Vis spectroscopy, X-ray diffraction (XRD), and scanning electron microscopy (SEM) were used to gain a better understanding of the size and morphology of nanoparticles (NPs) (Hayward et al., 2020).

Antifungal assay using well diffusion assay

The antifungal assay was conducted with *Candida* albicans and *Aspergillus niger*. A pour plate method was used to perform antifungal well diffusion assay. One percent of active fungal cultures were inoculated into sterilized agar media immediately before the media solidified,

and then the mixture was poured into the Petri plates. The culture of *candida* was inoculated into agar medium, while the spores of *Aspergillus* were extracted from sterile saline and mixed with potato dextrose media. Antibiotic of 1% (*Streptomycin/Chloramphenicol*) was added to the media just before pouring into the plates to prevent bacterial contamination. Following the plates' solidification, sterile well borer holes were bored into them, and 100 µl of metal nanoparticles sample material in various concentration was inserted into each hole. For *candida*, the plates were incubated at 37 °C for 18–24 hours, and for *Aspergillus,* they were incubated at 25 °C for 96 hours. After that, the findings were recorded.

Antibacterial assay using well diffusion assay

The process of making active cultures begins with moving one pure culture colony into a 150 ml conical flask that already contains 50 ml of the appropriate culture medium (e.g., nutrient broth, Yeast Extract Peptone Dextrose broth, or Tryptone soy broth). The flask is then placed in an incubator at 37 °C for 8–12 hours to activate and allow the culture to grow. Before making aliquots of varying concentrations for the Minimum Inhibitory Concentration (MIC) experiment, powdered compounds are dissolved in 1 ml of a suitable solvent like water, methanol, or DMSO. The concentrations needed for testing can be achieved by diluting liquid samples with water or solvent or using them directly. *Staphylococcus aureus* and *Escherichia coli* are used as bacterial pathogens in the well diffusion method-based antibacterial assay. As the slurry is about to solidify, it is combined with autoclaved agar media containing 1% active bacterial cultures and then poured into Petri plates. Once the material is solidified, sterile well borers are used to drill holes in the media. Then, 100 µl samples with varying concentrations (50, 100, 150, 200 and 250 µg) are poured into each hole. After that, a bacterial incubator is used to keep the plates at 37 °C for 18 to 24 hours. After the incubation period, the tested samples are evaluated for their antibacterial activity against the bacterial pathogens by looking for zones of inhibition around the wells on the plates. The efficiency of the samples against the strains of bacteria being studied is evaluated by recording and analysing the observed results.

Photocatalytic degradation

Photocatalytic degradation is an advanced oxidation process used to degrade pollutants characterized by high concentration, complexity, and low biodegradability (Al Taie and Ozcan, 2024). This process harnesses light energy to drive the degradation of pollutants. For the photocatalytic degradation of Rh-B dye, a protocol was followed wherein 0.2 mg of Rh-B dye was dissolved in a 100 mL volumetric flask to create a 100 ppm solution. A 10 mL aliquot of this solution was further diluted with distilled water in a separate 100 mL volumetric flask to achieve a 10 ppm concentration, which served as the stock solution for subsequent studies. Photocatalytic experiments were conducted in a phyoto catalytic reactor (Bujnakova et al., 2017). Photocatalytic degradation studies involved testing Rhodamine dye concentrations of 0.1 mg, 0.2 mg, and 0.3 mg in the presence of MgS NPs and FeS NPs as catalysts at various time intervals of exposure. Samples were collected regularly to monitor dye degradation using UV-Vis spectroscopy.

RESULTS AND DISCUSSIONS

The UV-Visible absorption spectra of magnesium sulfide nanoparticles (MgS NPs) and ferrous sulfide nanoparticles (FeS NPs) were examined at ambient temperature with a UV-1800 instrument (Figure 1). The nanoparticles were created using an extract of *Hordeum vulgare* leaves. The spectral response of nanoparticles was evaluated by mixing the nanoparticle solution with distilled water and measuring the resulting mixture's absorption of light in the range of 200 to 800 nm (Chormey et al., 2023).

The research found that the absorption spectra of selected NPs were between 200 and 800 nm. It was by following a curve that started at the origin that the band gap became apparent. Due to its perfectly linear structure, the magnesium sulfate nanoparticles being considered are highly suitable for use as direct band materials. A highly appealing characteristic of the MgS and FeS NPs is their semiconducting band gap, which was found to be 2.0 eV. Nanoparticles of metal sulfide show a high level of crystallinity when they have an emission band gap that is well-defined. Because, excitons are only embedded in the presence of nanoparticles, the quantum confinement effect causes the band gap to shift to the blue, indicating
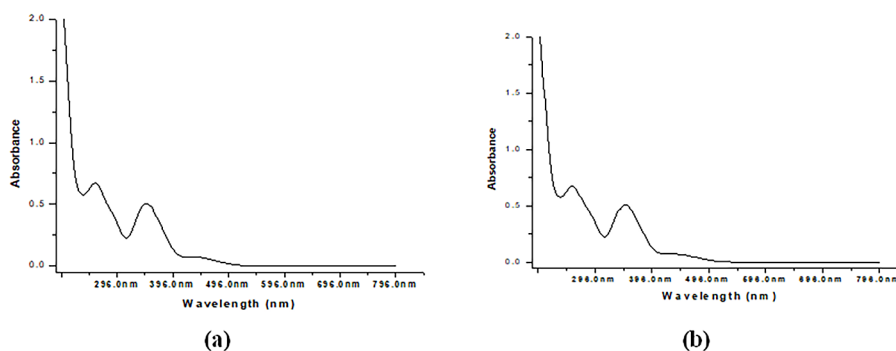
Figure 1. UV-Vis spectra of *Hordeum vulgare* capped (a) MgS NPs and (b) FeS NPs

the presence of nanoparticle materials. Figure 1 is a graph shows the absorbance-wavelength connection for MgS NPs and FeS NPs. Nanoparticles absorb more light when their band gap is larger. When the band gap amplitude increases, it means that nanoparticles (NPs) are present. The increase is due to the fact that electrons and holes are contained inside a small spatial region. Nanoparticles (NPs) may hasten the photocatalytic degradation of textile dyes due to their enhanced absorption of visible light. The X-ray diffraction (XRD) pattern of magnesium sulfide nanoparticles (MgS NPs) produced from an extract of *Hordeum vulgare* leaves showed separate diffraction peaks at 35.04, 50.1, and 60.2 degrees, corresponding to different crystal planes. The positions of these peaks show a strong relationship with earlier literature (El Sheekh et al., 2022). These revealed that spherical structures made up of numerous crystals organized in a monoclinic pattern. According to the graphic, the majority of the particles were orientated between 50 and 60 planes. The typical crystal size was found that an average size of 14 nm for MgS and FeS NPs (Elizabeth et al., 2022). The diffraction pattern demonstrates that the produced MgS and FeS NPs have a crystalline structure, as illustrated in Figure 2.

SEM can examine milligrams of material to detect particle size, shape, and surface qualities (Afsheen et al., 2020). It produces comprehensive images that show the spatial diversity of features within a particular area. At a voltage of 15 kV, the sample of MgS NPs and FeS NPs was evaluated under various magnifications and scale bars. The morphology was analyzed at various magnifications (5000x, 10,000x, 20,000x, 2500x, 60,000x, and 40,000x) and places. The SEM images showed that most MgS NPs convert into spherical clusters during assembly. It pictures rarely showed particles as small as 10 nm, indicating a size range of 10 to 50 nm. Figure 3 (a) and (b) of the SEM images indicate, as per West (2022), that the magnesium sulfide nanoparticles (MgS NPs) are present in a range of morphologies, including spherical, rod, bean-like, and other non-standard forms. In most cases, the size and distribution of particles remain constant. Capping *Hordeum vulgare* with MgS nanoparticles makes it very reactive and small.

Figure 4 illustrate FeS NPs with various morphologies, in the form of bean, spherical, rod-like, and other irregular shapes, indicating diversity in particle structure. The SEM photos depict the process of aggregation of FeS NPs, demonstrating
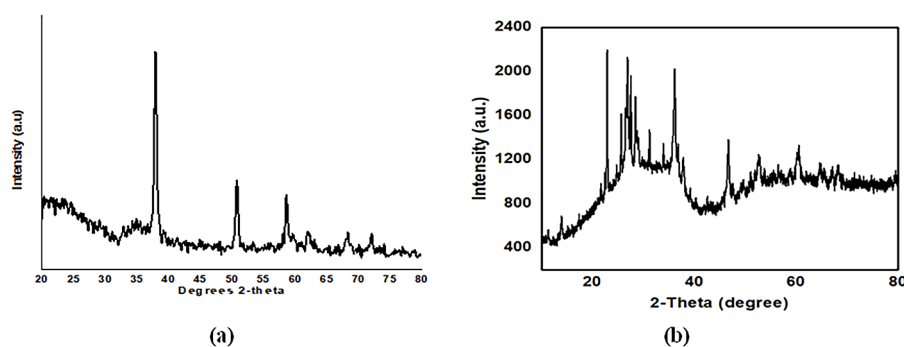
Figure 2. XRD pattern of *Hordeum vulgare* capped (a) MgS NPs and (b) FeS NPs
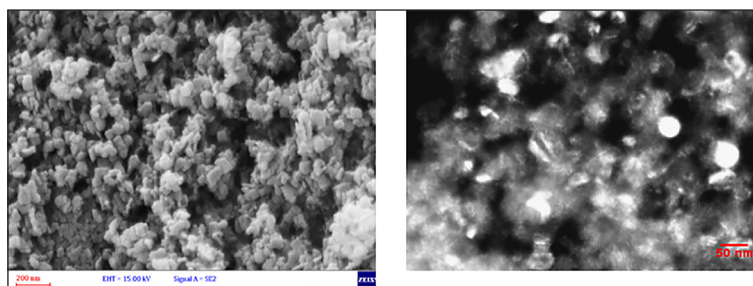
Figure 3. SEM images of *Hordeum vulgare* capped MgS NPs
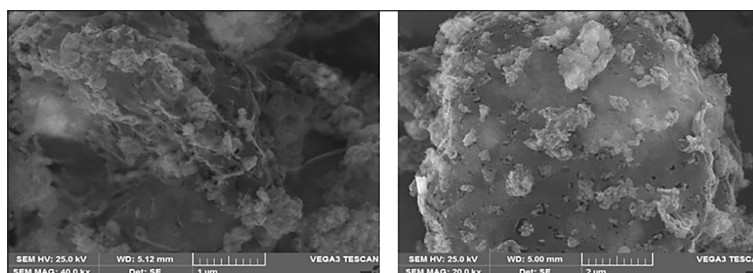
Figure 4. SEM Images of *Hordeum vulgare* capped FeS NPs

that the majority of the nanoparticles form spherical aggregates. 500 nm particles were discovered, which is consistent with previous research indicating a size range of 500 nm. SEM pictures in Regardless of their varied shapes, the particles consistently display specific dimensions and distributions, which offer valuable information about the morphology and properties of FeS NPs during the process of aggregation.

Antimicrobial activity

The produced FeS NPs and MgS NPs were evaluated for their antibacterial efficacy against human pathogenic bacteria, specifically *E. coli* (Gram-negative) and *S. aureus* (Gram-positive), using the agar well diffusion method. The

bacterial strain was inoculated into nutrient agar plates using aseptic techniques. Different concentrations (50 μg, 100 μg, 150 μg 200 μg and 250 μg) of FeS NPs and MgS NPs were pipetted into 7 mm diameter wells for incubation. The zone of inhibition, measured in millimetres (mm), was determined and recorded after the incubation period. The results are presented in Table 1. The experiments were conducted three times to ensure accuracy and reliability. The chloramphenicol, gentamicin, and cefalexin were employed as control agents (Weiss & Moser, 2015). The plates were examined following the incubation time and the findings were recorded. The antibacterial activity of FeS NPs and MgS NPs was assessed by determining their minimum inhibitory concentrations (MIC) (Figure 5 and 6).

Table 1. Observation of zone of inhibition of metal nanoparticles of *Hordeum vulgare*

| Pathogen | Sample | Zone of inhibition (mm) at different concentrations (μg) | | | | | MIC (μg) |
		50	100	150	200	250	
S. aureus	FeSNP	-	-	-	08	09	200
	MgSNP	-	-	-	-	-	-
E. coli	FeSNP	-	-	-	08	09	200
	MgSNP	-	-	-	-	-	-
C. albicans	FeSNP	-	-	-	08	09	200
	MgSNP	-	-	-	08	09	200
A. Niger	FeSNP	-	-	-	08	09	200
	MgSNP	-	-	-	07	08	200
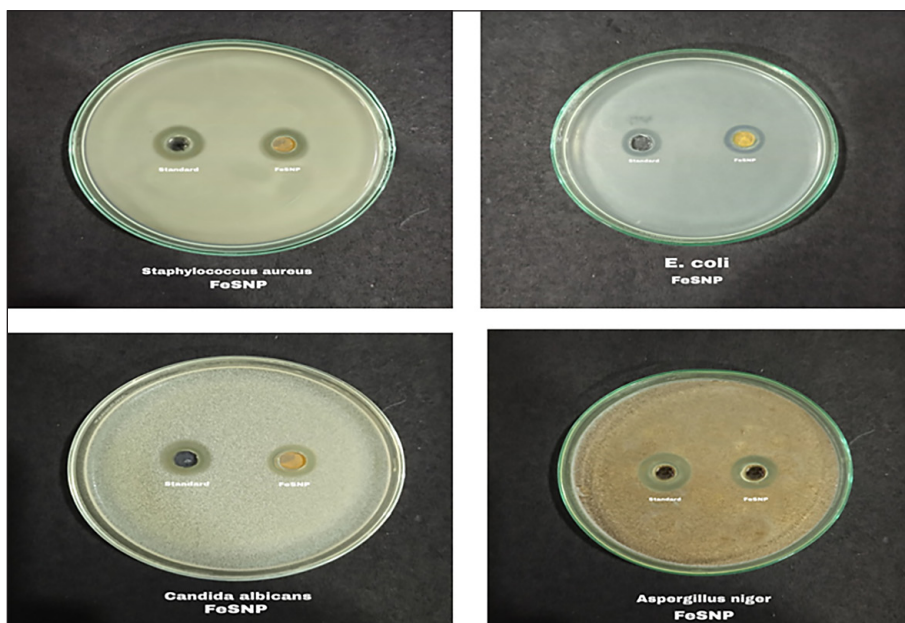
Figure 5. Zone of inhibition FeSNP
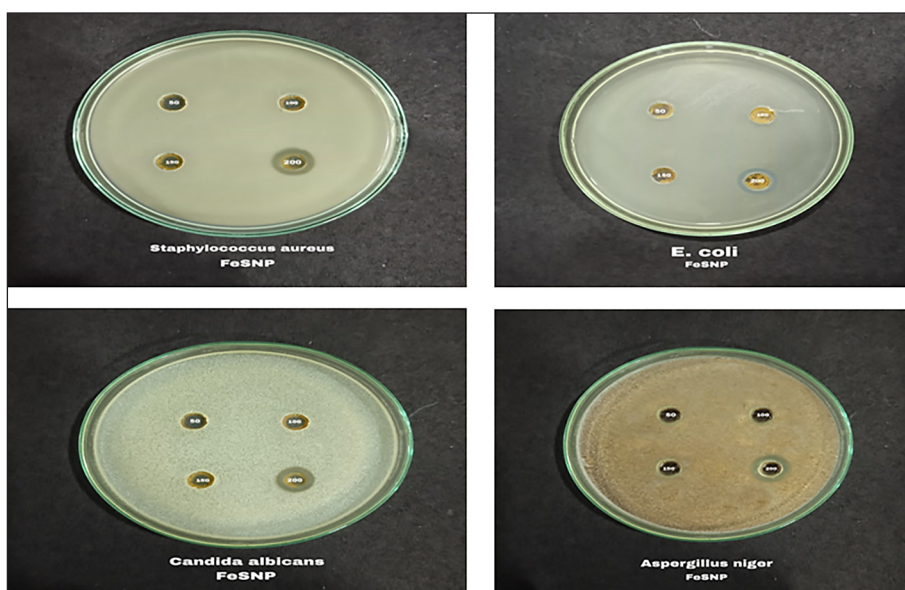
Figure 6. Zone of inhibition MgS NP

The MIC value was determined to be 200 µg. In contrast, the MgS NPs did not indicate any zone of inhibition against *E. coli* and *S. aureus*. The Antifungal assay was conducted using FeS NP and MgS NP against *C. albicans* and *A. niger*. The antifungal activity of the samples was evaluated using the well diffusion assay. This was done by incorporating 1% of active fungal cultures into autoclaved agar media immediately before it solidified. As for *A. niger*, spores were collected in sterile saline and then placed to potato dextrose media before being poured. Prior to transferring the solution onto the plates, 1% antibiotic (either *Streptomycin* or *Chloramphenicol*) was introduced into the media in order to prevent any bacterial contamination. Once the plates had hardened, sterile well borers were used to create wells. Subsequently 100 µl samples were placed into each of the wells. The plates were placed in an incubator at a temperature of 37 °C for a duration of 18–24 hours to cultivate *C. albicans*, and at a temperature of 25 °C for a duration of 96 hours to cultivate *A. niger*. The FeS NPs exhibited a zone of inhibition against both *C. albicans* and *A. niger* at dosages of 200 µg and 250

μg, with measurements of 08 mm and 09 mm, respectively (Figure 7). The MIC value was found to be 200 μg. In addition, MgS NPs has demonstrated a zone of inhibition against *C. albicans*, with MIC values of 200 μg. At dosages of 200 μg and 250 μg, the corresponding inhibition zone diameters were measured at 08 and 09 mm, respectively (Figure 8). However, MgS NPs exhibited a zone of inhibition against *A. Niger*, with measurements of 07 mm and 08 mm at dosages of 200 μg and 250 μg, respectively, and a MIC value of 200μg.

The antimicrobial activity of metal nanoparticles proves as an effective alternative for combating antimicrobial drug resistance. Similarly it was observed that at a concentration of 200 μg both MgS NPs and FeS NPs were effective on fungal strains and FeS NPs were observed to be efficient at a low dose of 200 μg on both bacteria and fungi. This variation in the inhibition rate is by the maximum alteration of the nanoparticles that occurred by the green synthesis of metal sulfide nanoparticles from *Hordeum vulgare* leaf extract.
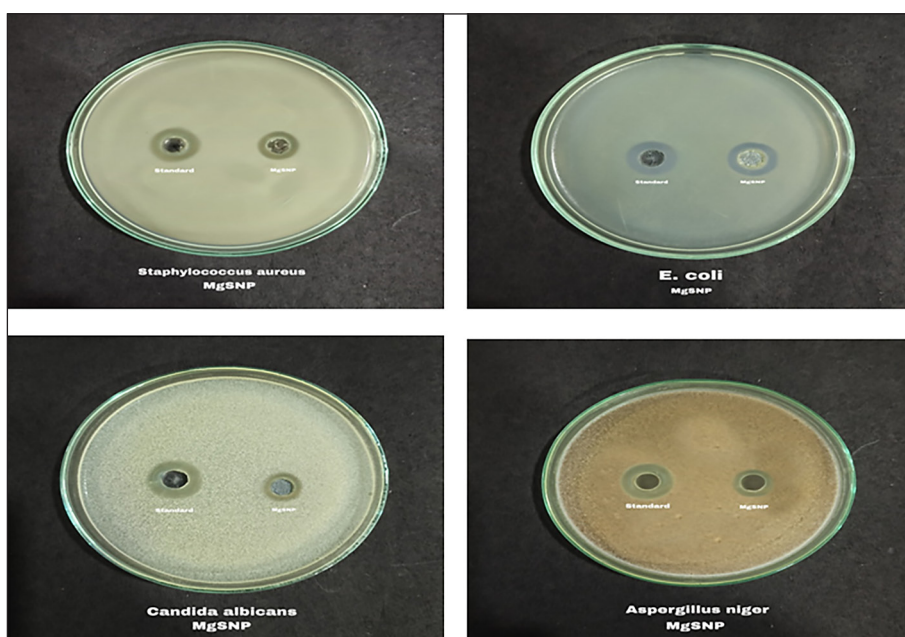
Figure 7. MIC of FeSNP
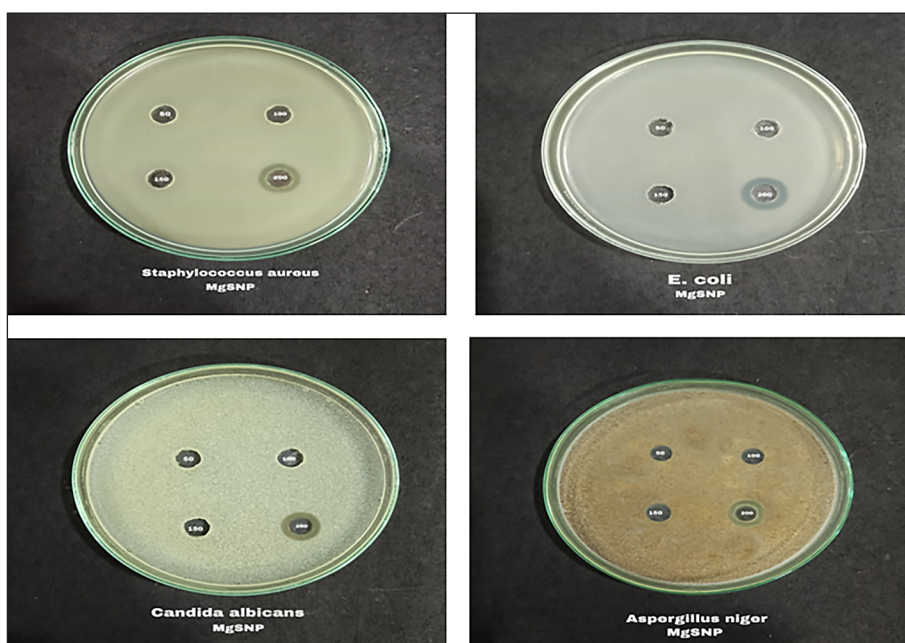
Figure 8. MIC of MgSNP

Table 2. Photocatalytic degradation studies using MgS NP at different concentrations of catalyst

S. No.	Catalyst	Concentration of catalyst	Dye degradation (%)
1	FeSNP	5	4
2	FeSNP	7.5	10
3	FeSNP	10	18
4	FeSNP	12.5	14
5	FeSNP	15	12
6	FeSNP	20	5

Photocatalytic degradation

The photocatalytic degradation of Rhodamine B (Rh-B) dye using MgS NPs and FeS NPs were investigated under UV irradiation, varying the concentrations of FeS NPs as the photocatalyst. Initially, the mixture of Rh-B dye and FeS NPs was stirred in the dark for 30 minutes to establish absorption-desorption equilibrium. Subsequently, the mixture was exposed to UV light with varying concentrations of MgS NPs and FeS NPs over a 3-hour duration. The change in Rh-B dye concentration was recorded at 30-minute intervals using a UV-visible spectrophotometer, with a maximum absorbance at 553 nm. To monitor the photocatalytic degradation, 6 ml of the mixture was collected at 30-minute intervals, centrifuged at 3000 rpm for 5minutes, and analysed using UV-Vis spectrophotometry at 553 nm. Initial and final Rh-B concentrations were determined using a calibration curve established for Rh-B concentrations ranging from 1 mg/L to 15 mg/L. The experimental data, including initial and final concentrations, were recorded and tabulated for analysis. This study evaluated the efficacy of phyto capped FeS and MgS nanoparticles as photocatalysts for RhB dye degradation under UV light exposure are shown in Table 2.

Based on the photocatalytic degradation study, it was determined that FeS nanoparticles (FeS NPs) at concentrations of 7.5 mg and 10 mg were effective in degrading Rhodamine dye, with observed degradation percentages indicating their photocatalytic activity. Specifically, 7.5 mg of FeS NPs achieved a 10% reduction in Rhodamine dye absorbance, while 10 mg of FeS NPs achieved an 18% reduction over the monitored time intervals. Conversely, concentrations of 5 mg, 12.5 mg, and 15 mg of FeS NPs were found to be less effective in degrading the dye based on the photocatalytic studies. The percentage of dye degradation was calculated using UV-Vis spectroscopy at 30-minute intervals, where the reduction percentage was determined by comparing initial (A_o) and subsequent (A_t) absorbance values. These findings suggest that FeS nanoparticles are effective at low concentration in dye degradation can and serve as effective alternatives for sustainable treatment of textile wastewater, and there by demonstrate promising potential for environmental remediation applications (Wang et al., 2024).

The photocatalytic degradation of Rhodamine dye was significantly enhanced in the presence of MgS nanoparticles (MgS NPs), with the optimal catalyst concentration identified as 40 mg in 0.2 mg/100 mL of Rhodamine dye solution, achieving maximum degradation. This concentration of catalyst demonstrated promising results, achieving up to 95% degradation of the dye after a 3-hour exposure period. The high surface area of metal sufide nanoparticles contributes to their enhanced photocatalytic activity, making them effective catalysts for dye degradation. Given the non-biodegradable nature of textile dye effluents and their environmental impacts, the use of MgS NPs as catalysts for bioremediation shows eco-friendly approach for textile wastewater treatment. This method offers a potential solution to address the challenges posed by textile industry effluents, highlighting a new pathway for sustainable wastewater treatment practices. This research work is at initial pilot scale study of developing a sustainable textile dye degradation still there is need for more research with different textile dyes to develop a sustainable environmental remediation for textile waste treatment.

CONCLUSIONS

Over the past two decades, there has been a growing emphasis on green chemistry and nanotechnology, driving the development of eco-friendly synthetic routes for nanomaterial synthesis using plants, microorganisms, and other

natural sources. This research utilized *Hordeum vulgare* leaf extract successfully to isolate MgS NPs, and FeS NPs which were characterized using UV-Vis analysis, XRD, and SEM techniques. The photocatalytic degradation of toxic Rhodamine dye by these metal sulfide nanoparticles demonstrated significant effectiveness, achieving 95% degradation with 40 mg of MgS NPs and 10 mg of FeS NPs, highlighting their potential for textile wastewater treatment through bioremediation. Additionally, the metal sulfide nanoparticles exhibited antimicrobial activity against both bacteria (*Staphylococcus, E. coli*) and fungi (*Aspergillus, Candida albicans*), suggesting their potential in addressing issues related to multi-drug-resistant microbes. This research opens up several progressive research avenues for metal sufide nanoparticles in sustainable environmental applications, providing opportunities for further research and development in this promising field.

REFERENCES

1. Afsheen S., H. Naseer, T. Iqbal, M. Abrar, A. Bashir, M. Ijaz. (2020). Synthesis and characterization of metal sulphide nanoparticles to investigate the effect of nanoparticles on germination of soybean and wheat seeds. *Materials Chemistry and Physics*, *252*, 123216.

2. Agbasi J.C., A.L. Ezugwu, M.E. Omeka, I.A. Ucheana, C.C. Aralu, H.O. Abugu, J.C. Egbueri. (2024). More about making profits or providing safe drinking water? A state-of-the-art review on sachet water contamination in Nigeria. *Journal of Environmental Science and Health, Part C*, 1–43.

3. Alsaiari N.S., F.M. Alzahrani, A. Amari, H. Osman, H.N. Harharah, N. Elboughdiri, M.A. Tahoon. (2023). Plant and microbial approaches as green methods for the synthesis of nanomaterials: Synthesis, applications, and future perspectives. *Molecules, 28*.

4. Al-Taie A., E. Ozcan Bulbul. (2024). A paradigm use of monoclonal antibodies-conjugated nanoparticles in breast cancer treatment: current status and potential approaches. *J Drug Target, 32*, 45–56.

5. Azzazy H.M.E., Mansour M.M.H., Samir T.M., Franco R. (2012). Gold nanoparticles in the clinical laboratory: principles of preparation and applications. *Clin Chem Lab Med, 50*, 193–209.

6. Bujnakova Z., Dutkova E., Kello M., Mojzis J., Balaz M., Balaz P., Shpotyuk O. (2017). Mechanochemistry of Chitosan-Coated Zinc Sulfide (ZnS) Nanocrystals for Bio-imaging Applications, *Nanoscale Research Letters, 12*, 328.

7. Chormey D.S., Zaman B.T., Borahan Kustanto T., Erarpat Bodur S., Bodur S., Tekin Z., Nejati O., Bakırdere S. (2023). Biogenic synthesis of novel nanomaterials and their applications. *Nanoscale, 15*, 19423–19447.

8. Crocker J., Ogutu, E.A., Snyder, J., Freeman, M.C. (2024). The state of reporting context and implementation in peer-reviewed evaluations of water, sanitation, and hygiene interventions: A scoping review. *International Journal of Hygiene and Environmental Health, 259*, 114363.

9. Elizabeth K., Uma Devi R., Ratnamala A., Kumar M.S., Raja K.P. (2022). Biogenic synthesis and characterization of Metal Sulphide nanocomposites and its application to seed germination, *International journal of health sciences, 6*, 10266–10282.

10. El-Sheekh M.M., Morsi H.H., Hassan L.H.S., Ali S.S. (2022). The efficient role of algae as green factories for nanotechnology and their vital applications. *Microbiol Res, 263*, 2.

11. Forstinus N.O., Ikechukwu N.E., Emenike M.P., Christiana A.O. (2015). Water and waterborne Diseases: A review. *International Journal of TROPICAL DISEASE & Health, 12*, 1–14.

12. Gnat S., Łagowski D., Nowakiewicz A., Dyląg M. (2021). A global view on fungal infections in humans and animals: opportunistic infections and microsporidioses. *Journal of Applied Microbiology, 131*, 2095–2113.

13. Gul Z., Ullah S., Khan S., Ullah H., Khan M.U., Ullah M., Ali S., Altaf A.A. (2024). Recent Progress in Nanoparticles Based Sensors for the Detection of Mercury (II) Ions in Environmental and Biological Samples. *Crit Rev Anal Chem, 54*, 44–60.

14. Hamdaoui O. (2011). Intensification of the sorption of Rhodamine B from aqueous phase by loquat seeds using ultrasound. *Desalination, 27*, 279–286.

15. Hayward C., Ross K.E., Brown M.H., Whiley H. (2020). *Water as a Source of Antimicrobial Resistance and Healthcare-Associated Infections*.in. Pathogens.

16. Kaur N. (2024). An innovative outlook on utilization of agro waste in fabrication of functional nanoparticles for industrial and biological applications: A review. *Talanta, 267*, 125114.

17. Kinch M.S., Kraft Z., Schwartz T.. (2024). Antibiotic Development: Lessons from the Past and Future Opportunities, Pharmaceutical Research.

18. Nagaraja R., Kottam N., Girija C.R., Nagabhushana B.M. (2012). Photocatalytic degradation of Rhodamine B dye under UV/solar light using ZnO nanopowder synthesized by solution combustion route. *Powder Technology*, 215–216, 91–97.

19. Nanda A., Pandey P., Rajinikanth P.S., Singh N. (2024). Revolution of nanotechnology in food packaging: Harnessing electrospun zein nanofibers for improved preservation – A review. *Int J Biol*

Macromol, 13, 129416.

20. Qin X., Ding L., Hao M., Li P., Hu F., Wang M. (2024). Antimicrobial resistance of clinical bacterial isolates in China: current status and trends. *JAC-Antimicrobial Resistance, 6*.

21. Richardson S.D., Willson C.S., Rusch K.A. (2004). Use of rhodamine water tracer in the marshland upwelling system. *Groundwater, 42*, 678–688.

22. Sharma P., Ganguly M., Sahu M. (2024). Role of transition metals in coinage metal nanoclusters for the remediation of toxic dyes in aqueous systems.

RSC Advances, 14, 11411–11428.

23. Wang C., Sun S., Wang P., Zhao H., Li W. (2024). Nanotechnology-based analytical techniques for the detection of contaminants in aquatic products. *Talanta, 269*, 25.

24. Weiss C.A., Moser R. (2015). *Sample preparation of nano-sized inorganic materials for scanning electron microscopy or transmission electron microscopy.* Scientific Operating Procedure SOP-P-2.

25. West A.R. (2022). Solid state chemistry and its applications. 2nd Edition.